The Atmospheric Oxidizing Capacity in China: Part 2. Sensitivity to emissions of primary pollutants

Jianing Dai[a], Guy P. Brasseur[a,e,f], Mihalis Vrekoussis[b,g,h], Maria Kanakidou[b,d], Kun Qu[b], Yijuan Zhang[b], Hongliang Zhang[c], Tao Wang[f]

[a] Environmental Modelling Group, Max Planck Institute for Meteorology, Hamburg, 20146, Germany
[b] Institute of Environmental Physics (IUP), University of Bremen, Bremen, 28359, Germany
[c] Department of Environmental Science and Engineering, Fudan University, Shanghai, 200433, China
[d] Environmental Chemical Processes Laboratory, Department of Chemistry, University of Crete, Heraklion, 70013, Greece
[e] National Center for Atmospheric Research, Boulder, Colorado, 80307, USA
[f] Department of Civil and Environmental Engineering, The Hong Kong Polytechnic University, Hong Kong, China
[g] Center of Marine Environmental Sciences (MARUM), University of Bremen, Bremen, 28359, Germany
[h] Climate and Atmosphere Research Center (CARE-C), The Cyprus Institute, Nicosia, Cyprus

Correspondence to: Guy P. Brasseur (guy.brasseur@mpimet.mpg.de)

Abstract

The Atmospheric Oxidation Capacity (*AOC*), often referred to as the self-cleansing ability of the atmosphere, considerably affects the concentrations of photochemical air pollutants. Despite substantial reductions in anthropogenic emissions of key chemical compounds in China, the mechanisms that determine the changes in the atmospheric oxidation capacity are still not sufficiently understood. Here, a regional chemical transport model is employed to quantify the sensitivity of air pollutants and photochemical parameters to specified emission reductions for winter and summer conditions (January and July 2018). The model simulations show that, in winter, a 50% decrease in nitrogen oxide (NO_x) emissions leads to an increase of 6-12 ppbv (15-33%) in surface ozone (O_3) concentrations across China. In summer, the O_3 concentration decreases by 2-8 ppbv (3-12%) in NO_x-limited areas, while it increases by up to 8 ppbv (17%) in volatile organic compounds (VOCs)-limited areas. This O_3 increase is associated with a reduced NO_x-titration effect and with higher levels of hydroxyl (OH) and hydroperoxyl (HO_2) radicals due to a reduced loss by reactions with nitrogen dioxide (NO_2) and by a decreased aerosol uptake. With an additional 50% reduction in anthropogenic VOCs emissions, the O_3 concentration decreases by 5-12 ppbv (6-15%) in the entire geographic area, with an exception in the regions, where the role of BVOCs is crucial to ozone formation. Further, the adopted reduction in NO_x emission leads to an increase of *AOC* by 18% in VOC-limited areas. This specific increase is associated with the enhanced radical cycles from the photolysis of oxidized VOCs (OVOCs) and the oxidation of alkenes by OH radicals and O_3. This study highlights that the photolysis of OVOCs and the oxidation of alkenes and aromatic compounds in urban areas promote an increase in O_3 when the NO_x emissions are reduced. To mitigate O_3 rises in urban areas, a joint reduction in the emission of NO_x and in specific VOCs species, including alkenes, aromatics, and unsaturated OVOCs, including methanol and ethanol, should be implemented.

Keywords: ozone pollution, emission reduction, nitrogen chemistry, *AOC*

1. Introduction

To effectively reduce air pollution in China, the government of the country has implemented stringent actions between 2013 and 2020 (Liu et al., 2020; Liu et al., 2023). In the initial phase, from 2013 to 2017, the control of primary pollutants was particularly effective, with a dramatic decrease in the anthropogenic emissions of fine particles ($PM_{2.5}$), sulfur dioxide (SO_2), and nitrogen oxides (NO_x) (Zheng et al., 2018; Liu et al., 2020). In subsequent years, a sustained reduction in the emission of SO_2, NO_x, and $PM_{2.5}$ was achieved, particularly between 2018 and 2020 (Liu et al., 2023). The implementation of the emission control policies has greatly improved China's air quality. However, a significant increase in the surface ozone (O_3) concentration was observed from 2013 to 2019, with the positive trend slowing down in 2020 and 2021, but rebounding in 2022 (Liu et al., 2023; China Air 2023). Several studies provide explanations for the positive trend observed in the surface O_3 concentration, including a reduction in NO_x emissions and in the atmospheric aerosol loading (Li et al., 2019; Liu et al., 2020). During and after the recent COVID-19 lockdown period, ozone pollution has been reported to happen, which is believed to be favored by the sharp reduction of NO_x and high emissions of volatile organic compounds (VOCs) (Li et al., 2021). Looking through these changes over the past decade, we learn that rapid reductions of emissions disturb the current ozone chemistry and, thereby, produce changes in the ozone concentrations.

The response of ozone to reduced NO_x emissions varies with the local photochemical environment and specifically with the chemical regimes (i.e., VOC-limited, NO_x-limited, or transition conditions) (Jacob., et al., 1995; Ou et al., 2016; Dai et al., 2023). In NO_x-sensitive regimes, the reduction in NO_x emissions decreases the amount of NO_2 molecules photolyzed, leading to fewer ozone molecules being produced. While, in VOC-sensitive regimes, the reduction in the NO_x abundance tends to enhance the ozone formation due to the weakening of NO titration and the reduced loss of OH radical reacted with NO_2. Several studies based on satellite observations (Wang et al., 2021) and regional models (Zhu et al., 2023) have shown that the reduction in anthropogenic emissions has generated a change in the geographical distribution of the ozone formation regimes in China. These studies have reported a shift of ozone sensitivity regimes from VOC-sensitive to transition and/or NO_x-sensitive in many metropolitan and suburban regions of East China. The shift towards NO_x-limited conditions facilitates the implementation of an efficient ozone control through the reduction in NO_x emissions only. In the remaining VOC-sensitive and transition areas, NO_x emission reduction fails to effectively mitigate ozone pollution. In this situation, a coordinated reduction in anthropogenic VOCs (AVOCs) emissions should be implemented to effectively limit the ozone formation (Liu et al., 2023; Zhu et al., 2023). The source of NO_x in VOC-sensitive areas is mainly from fossil fuel combustion, while the emissions of AVOCs emissions result from a broad range of industrial, transportation and residential sources (B. Li et al., 2021; C. Li et al., 2022). To establish a cost-effective control over AVOCs emissions, the contribution of different VOCs categories to ozone formation should be accurately accessed for different areas of China.

The effect of aerosols on the O_3 formation has been considered in several modeling studies (Li et al., 2019; Liu et al., 2020). However, the influences of aerosol on the O_3 production are complex due to the different effects to be taken into consideration. (Tan et al., 2022; Dai et al., 2023). Understanding the changes in aerosol effects on the O_3 formation when the primary emissions are further reduced remains a necessary condition for implementing efficient air quality control policies.

Recent observational studies combined with a source apportionment approach using observation-based models have highlighted the role of anthropogenic VOCs species, including the alkenes, aromatics, and oxidized volatile organic compounds (OVOCs), in mitigating summertime ozone formation in urban areas in China (C. Li et al., 2022; W. Wang et al., 2023) regions. The notable contributions of OVOCs to the oxidizing capacity of the atmosphere (*AOC*) as well as the formation of secondary organic aerosols (SOA) have been of concern in the regions of Yangzi River Delta (YRD) (J. Li et al., 2022) and Pearl River Delta (PRD) (W. Wang et al., 2022). The important role of biogenic VOCs (BVOCs) has also been highlighted in vegetated rural and urban regions in China, since the oxidation of BVOCs can significantly contribute to the formation of ozone and aerosols in the PRD region (J. Wang et al., 2023; Zhang et al., 2023). However, a comprehensive evaluation of the changes in the contribution of different VOCs categories to *AOC* and in ozone chemistry due to the emission changes in different regions of China is still needed. Considering the necessity of implementing coordinated actions among large areas to further alleviate air pollution in China, regional chemical transport models are appropriate tools to assess the quantitative response of the formation of secondary pollutants and of the oxidizing capacity of the atmosphere to emission changes.

In the companion paper (Part 1; Dai et al., 2023), we used a regional chemical-meteorological model to quantify the relative contribution of different photochemical processes to the formation and destruction of near-surface photochemical radicals and ozone in different chemical environments in China. In Part 2 of the study, with the evaluated model, we assess the response of the photo-oxidative species and related parameters to an imposed reduction of primary emissions. This paper is structured as follows. Section 2 introduces the setups of the model system and describes the simulations performed for specified reductions in the emissions of primary pollutants. In Section 3, we first analyze the response in the near-surface concentration of ozone precursors and intermediate to primary emission reduction. We also discuss the changes in the ozone formation regime. Further, we derive the associated changes in ozone and aerosols to the emission reduction. Finally, we describe the sensitivity of the atmospheric oxidative capacity (*AOC*) to the reduction in emissions. A summary and implication for policy making of our study is provided in Sec. 4.

2. Method

2.1. Model setting

We use the WRF-Chem model version 4.1.2 (Skamarock et al., 2019), coupled with the gas-phase chemistry mechanism MOZART (Emmons et al., 2010) and the aerosol module MOSAIC (Zaveri et al., 2008), to simulate the meteorological fields as well as the transport, the chemical and physical transformations of trace gases and aerosols. The months of January and July of 2018 were selected as representative months to conduct the simulations and to investigate the changes in secondary pollution and in the *AOC* in response to emission reductions during winter and summer, respectively. Compared to the standard version of the chemical mechanism, several updates of heterogeneous uptake on the surface of the ambient aerosol were implemented (Dai et al., 2023). As for the SOA formation, the main pathways result from the gas-phase oxidation of VOCs by atmospheric oxidants (OH, O_3, and NO_3) and from the heterogeneous formation of glyoxal SOA over the ambient aerosol (Knote et al., 2014). The model domain covers the whole geographical area of China. Analyses of modeling results at four urban sites (Beijing, Shanghai, Guangzhou, and Chengdu) were also performed. More detailed information on the model configuration, the model validation, and the sites selected for our analysis can be found in Part 1 of our paper Dai et al., (2023).

We adopt the Multi-resolution Emission Inventory (MEIC v1.3; http://www.meicmodel.org/) to represent anthropogenic emissions in China and the CAMS-GLOB-ANT v4.2 inventory (https://eccad.aeris-data.fr/) provided by the Copernicus Atmosphere Monitoring Service (CAMS) to account for the anthropogenic emissions in the Asian areas outside China. To explore the sensitivity of secondary pollution and of *AOC* to emission reduction, several sensitivity experiments were designed based on our emissions inputs of NO_x, anthropogenic VOCs (AVOCs). As shown in Table S1 of the Supplementary Information, NO_x emissions include the emissions of NO_2 and NO, AVOCs emissions include those of alkanes [ethane (C_2H_6), propane (C_3H_8), and BIGALK (alkanes with carbon number $\geqslant$ 4)], alkenes [ethene (C_2H_4), propene (C_3H_6), and BIGENE (alkenes with carbon number$\geqslant$4)], aromatics [benzene (C_6H_6), toluene ($C_6H_5CH_3$), and xylene ($C_6H_4(CH_3)_2$))], alkyne (C_2H_2), isoprene (C_5H_8), terpenes ($C_{10}H_{16}$), and OVOCs [methanol (CH_3OH), ethanol (C_2H_5OH), acetaldehyde (CH_3CHO), acetone (CH_3COCH_3), methacrolein (CH_2CCH_3CHO; MACR), and methyl vinyl ketone ($CH_2CHCOCH_3$; MVK)]. The emissions of ammonia (NH_3), sulfur dioxide (SO_2), and carbon monoxide (CO) are also considered.

2.2. Design of numerical experiment

To explore the sensitivity of secondary pollutants to emissions changes, five numerical experiments are conducted for January and July of 2018, respectively (Table 1). In the baseline case, denoted as "*BASE*", we adopted the emissions described in Sect. 2.1. The concentrations of the key species calculated in this specific case have been validated in our companion study (Dai et al., 2023). To quantify the sensitivity of pollutants to potential mitigation policies, we apply uniform reductions in the surface emissions of primary pollutants over the entire geographical area of China; In the first two cases, arbitrary 50% reduction are applied separately in NO_x and AVOCs emissions relative to the baseline case. These two cases are labeled "*NO_x*" and "*AVOCs*", respectively. A third case in which the 50% reduction is applied to both NO_x and AVOCs emissions is referred to as "*N+A*". The difference between the

"perturbed" concentrations of pollutants and chemical parameters relative to the baseline case provides an estimate of the response in secondary pollution and chemistry to emission reduction.

Additionally, a simulation labeled "*TOTAL*" assumes that all anthropogenic emissions under consideration (NO_x, AVOCs, CO, SO_2, and NH_3) are simultaneously reduced by 50%. This particular case is used to explore the impact on the ozone formation of a reduction in the emission of CO (an ozone precursor) and of SO_2 and NH_3 (as aerosol precursors). The spatial distribution of the emission fluxes changes for the different cases is shown in Fig. S1.

3. **Model results**

3.1. Changes in precursors and intermediates in ozone formation

First, we describe the changes in the surface concentration of ozone precursors and intermediates, including the hydroxyl (OH) radical, the hydroperoxyl (HO_2) radical, and specific oxidized volatile organic compounds (OVOCs) species in response to the reduction in surface emissions. To support the discussion on the radical changes induced by the emission reduction, we examine the changes in two specific parameters: the production rate of RO_x radicals ($P(RO_x)$) and the destruction rate of RO_x radicals ($D(RO_x)$) (Tan et al., 2019). The production rate of RO_x radicals ($P(RO_x)$ includes the photolysis of O_3, of nitrous acid (HONO), and of different OVOCs, and the ozonolysis of alkenes. The destruction rate of RO_x radicals ($D(RO_x)$) results from the termination reactions between different RO_x radicals and between RO_x radicals with nitric oxide as well as from the heterogeneous uptake of HO_2 on aerosol surfaces. Detailed model estimates of $P(RO_x)$ and $D(RO_x)$ can be found in Part 1 of the present study (Dai et al., 2023).

3.1.1. Changes in radicals

Winter conditions. Figure 1 displays the spatial distribution of the changes in the surface daytime (06:00-19:00 Local Standard Time) mixing ratios of OH and HO_2 radicals resulting from a 50% reduction in the NO_x, AVOCs, and combined NO_x and AVOCs emissions for January 2018. With the reduction in NO_x emissions (*NOx* case), the calculated mixing ratio of the surface OH radical is decreased in southern China by up to 40% (0.05 pptv; Fig. 1a), with a lower reduction in the central and western parts of the country. The decreases in the NO_2 concentration (Fig. S2a), resulting from the reduced NO_x emissions, lead to the reduced formation of ozone. As a result, the oxidation capacity and levels of oxidants are smaller than in the *BASE* case (see Sect. 3.3). At the same time, an increase in the concentration of the OH radical is found in urban areas, including the North China Plain (NCP), Yangzi River Delta (YRD), Pearl River Delta (PRD), and Si Chuan Basin (SCB) regions, with a maximum increase of 24% in the PRD region. This increase results from the reduced loss of the OH radical by the reaction with NO_2 (Fig. S2b). A distinct increase in the surface mixing ratio of HO_2 radical is derived in southern China (by up to 5 pptv or 60%; Fig. 1b). This enhancement is related to the increased mixing ratio of the OH radical found in urban areas, resulting in enhanced HO_2 levels

via VOCs oxidation, and a reduced HO_2 loss via the aerosol uptake, as the aerosol load is reduced (see Sect. 3.2.3) (Song et al., 2021).

For the 50% decrease in AVOCs emissions (*AVOCs* case), the mixing ratio of OH is reduced by 4-12% (0.005-0.015 pptv; Fig. 1c) and the mixing ratio of HO_2 radicals by 20-36% (1-3 pptv; Fig. 1d) in the southern part of China. The decrease in the mixing ratio of these radicals is related to the reduced oxidation rate of VOCs, due to the decrease in the concentration of hydrocarbons (Fig. S3a), whose emissions are reduced. The production of RO_x also decreases due to the reduced AVOCs emissions, especially from the photolysis of formaldehyde (HCHO), and other OVOCs (Fig. S3b-c). Simultaneously, a slight increase in the mixing ratio of OH radical is derived in the southern part of China. This increase in the OH radical is related to the reduced extinction of radiation associated with the decreased aerosol load due to the AVOCs emission reduction.

When the 50% emission reduction in NO_x is combined with the 50% reduction in AVOCs emissions (*N+A* case), the distribution of changes in the OH radical are similar to the pattern induced by emission reduction in NO_x alone. However, a weakened increase is calculated, as the increase in OH radical with reduced NO_x emissions is largely compensated by the decreased radical concentrations following the AVOCs emission reduction. As shown in Fig. 1e, the maximum increase in urban China is lowered to 12% (from 40%). The increase in the mixing ratio of HO_2 radicals is reduced to 20% (from 60%; Fig. 1f)), with only a mild increase distributed along the southern coast of China.

When accounting for the additional reduction in other anthropogenic emissions (NH_3, SO_2, and CO) (*TOTAL* case), the mixing ratio of the OH radical is positively modified, relative to the results in the combined case (*N+A* case). As shown in Fig. S4a, the mixing ratio of the OH radical is enhanced in the PRD and SCB regions (by up to 22%). This increase is due to the lowered consumption of the OH radical by the reduced concentration of carbon monoxide (CO) (Fig. S5a), due to its reduced emissions (Fig. S1d). For the HO_2 radicals, the additional reduction in the other emissions also contributes to a larger mixing ratio, with a pronounced increase in southern China (by up to 18%; Fig. S4c). This increase in the HO_2 radical mixing ratio is due to the increase in the oxidation of the VOCs by the OH radical and the reduced aerosol uptake of HO_2 associated with the decrease in the aerosol load.

Summer conditions. Figure 2 displays the spatial distribution of the changes in the surface daytime mixing ratio of the OH and HO_2 radicals due to the applied reduction in NO_x, AVOCs, and combined NO_x and AVOCs emissions for July 2018. Compared with the wintertime variation in radicals, which is limited to southern China, the geographical area covered by these summertime changes covers a larger fraction of China, including the northern provinces. When applying a 50% reduction in the NO_x emissions, the mixing ratio of the OH radicals decrease in large parts of China, with the maximum decrease reaching 40% (0.15 pptv; Fig. 2a). The concentration of the OH radical increases in the metropolitan areas, including in the YRD and PRD regions. Simultaneously, the surface mixing ratio of the HO_2 radical increases by 15-20% (6 to 8 pptv; Fig. 2d) in the North China Plain. These changes are affected by meteorological

parameters including the temperature, the water vapor abundance, and the solar radiation intensity, which affect the oxidative processes (Dai et al., 2023).

When AVOCs emissions are reduced by 50%, the mixing ratio of the radicals in urban areas, including in the NCP, YRD, and PRD regions, decreases on average by 8-12% in the case of OH (0.03-0.05 pptv; Fig. 2b) and by 6-10% in the case of HO_2 (3-5 pptv; Fig. 2e). When applying the combined 50% emission reduction in AVOCs and NO_x, the changes in the patterns of the OH radical are similar to the distribution derived for the reduction in NO_x emissions alone, but it is also partially offset by the counteracting effect of AVOCs emissions, as for winter conditions. As shown in Fig. 2c, the maximum increase in OH radical is reduced to 20% (from 40%) and the maximum decrease to 12% (from 30%). The counteracting effect of AVOCs emission reduction is also shown in the enhanced abundance of HO_2 radicals (Fig. 2f), with less than 6% (from 15-20%) increases in the urban areas.

With an additional 50% reduction in other anthropogenic emissions, the changes in OH and HO_2 radicals relative to the results in the combined case are smaller than the changes in winter conditions (Fig. S4b and d). This is due to the relevant small decrease in aerosol load during summer (see Sec. 3.2.3).

3.1.2 Changes in OVOCs

Oxygenated hydrocarbons (OVOCs) originate from direct biogenic and anthropogenic surface emissions (primary source), and from the oxidation of primary hydrocarbons (secondary source) in the atmosphere (W. Wang et al., 2022).

Winter conditions. Figure 3 shows the spatial distribution of the calculated changes in total OVOCs due to a 50% reduction in NO_x, AVOCs and in combined NO_x and AVOCs emissions for January of 2018. With the adopted reduction in NO_x emission, the OVOCs concentration decreases in the non-urban areas of southern China and increases in urbanized China (Fig. 3a), which is consistent with the changes derived for the mixing ratio of the OH radical. The highest increase in the OVOCs concentration is approximately10% (2 ppbv) in the urban areas of the YRD and PRD regions; it includes a significant increase in the concentration of formaldehyde (HCHO; Fig. S6a), followed by peroxyacetyl nitrate (PAN; Fig. S6b), and alcohols (CH_3OH and C_2H_5OH; Fig. S6c). At the four city sites under consideration, the highest increase in OVOCs is calculated at Shanghai and Guangzhou, with concentrations increasing by about 12% (1.8 ppbv; Fig. 3e) and 8% (1.2 ppbv; Fig. 3f), respectively.

When the AVOCs emissions are reduced, the abundance of OVOCs is reduced in most regions of China (Fig. 3b), with the highest decrease found in the regions of PRD and SCB. At the four city sites under consideration (Fig. 3d-g), the decrease is the most pronounced in the concentration of ketones, including acetone (CH_3COCH_3), methyl vinyl ketone ($CH_3C(O)CHCH_2$), and methyl ethyl ketone ($CH_3CH_3C(O)CH_2CH_3$). The abundance of these species is reduced by almost a factor of two, followed by HCHO and other aldehydes. When combining the emission reduction of AVOCs and NO_x, the decrease in OVOCs concentration

resulting from the AVOCs emission reduction is further strengthened in large parts of China (Fig. 3c). However, an increased mixing ratio of 1~2 ppbv is derived for OVOCs at the Guangzhou site (Fig. 3f), which is consistent with an increase in the mixing ratio of OH radical at this site (Fig. S7). With additional decreases in the other emissions, the OVOCs' concentration is enhanced by 2~4 ppbv in whole China (Fig. S4e), which is consistent with the increased abundance of the OH radical resulting from a reduction in the NH_3, SO_2, and CO emissions.

Summer conditions. Figure 4 displays the spatial distribution of the changes in total OVOC concentrations in response to a 50% reduction in NO_x, AVOCs and in the combined NO_x and AVOCs emissions for July 2018. With a 50% reduction in NO_x emissions, the changes in the OVOCs concentrations do not resemble the changes in the concentrations of the OH radical. A decrease in the OVOCs is derived in southern China. However, in central and northern China, the level of OVOCs generally increases and this increase is not limited to metropolitan areas (Fig. 4a). For specific OVOCs, the changes in HCHO, glyoxal, and PAN (Fig. S8a-c) are consistent with the changes calculated for the OH radical. However, for aldehydes and alcohols (Fig. S9a-b), an increased concentration is derived in the entire geographical area of China, with a consistent distribution of changes in alkenes (Fig. S9c) and isoprene (Fig. S9d). In summer, the temperature-dependent emissions of biogenic VOCs from vegetation are high (Zhang et al., 2023). The reduced production rate of OVOCs, resulting from the reduced AVOCs emissions, is compensated to a certain degree by the high natural emissions of BVOCs species.

With a 50% reduction in AVOCs emission, the OVOCs concentrations are significantly reduced in the NCP and SCB regions (Fig. 4b). Different from what is occurring in winter (OVOCs concentration reduced by about 50%), the response of the OVOCs to the AVOCs emission reduction is milder in summer, with the largest decrease being reduced to 30%. This is explained by the more effective secondary formation of OVOCs during summertime. Nevertheless, a more pronounced decrease in OVOC abundance is found in North China. For example, at the Beijing site, the decreases in OVOCs concentration reaches 10 ppbv compared to the 5 ppbv derived in winter, which is consistent with the higher concentration of summertime OVOCs (~34 ppbv) relative to winter (~11 ppbv). When the combined reduction in the emissions of AVOCs with NO_x are considered, a lower decrease of OVOCs is found in the geographical area of China (Fig. 4c), which is relevant to the reduced decrease in the OH concentration. The response on the OVOCs concentration to the reduced emissions applied to the other species under consideration is small (Fig. 4Sf).

3.2. Changes in secondary pollutants to emission reduction

The formation of ozone and secondary aerosol is affected by the changes in the emissions of primary organic species and in the concentration of ozone precursors and intermediate species. In order to highlight the regional differences in the response of the existing photochemical regimes to emission reduction, we first show the changes in the distributions of the areas where the ozone formation is either NO_x- or VOC-limited. We distinguish the two regions from the

calculated ratio between the production rate of hydrogen peroxide (H_2O_2) and of nitric acid (HNO_3) [$P(H_2O_2)/P(HNO_3)$]. An area is assumed to be VOC-limited or NO_x-limited if the adopted indicator $P(H_2O_2)/P(HNO_3)$ is smaller than 0.06 or if it is larger than 0.2, respectively (Tonnesen and Dennis, 2000; Yang et al., 2020; Zhao et al., 2019). The regions with ratios between these two limits represent transition situations. The production rate of odd oxygen (O_x = O_3 + NO_2), associated with recurrent radical reaction chains involving the oxidation of hydrocarbons in the presence of NO_x ($P(O_x)$), and the photochemical destruction rate of O_x ($D(O_x)$), is also adopted here to support the analysis of the underlying reasons for the calculated ozone changes. The detailed definition of $P(O_x)$ and $D(O_x)$ can be found in Dai et al., (2023).

3.2.1 Response of ozone sensitivity regimes to emission reduction

Figure 5 displays the spatial distribution of ozone regimes in response to applied emission reductions for the emissions of NO_x, AVOCs and for combined NO_x and AVOCs emissions in January and July.

Winter conditions. In January, with a 50% reduction in NO_x emissions, the regions characterized by transition or VOC-limited regimes in the south and southwest of China (in *BASE* case; Fig. 5a) tend to be converted into NO_x-limited areas regarding ozone production (Fig. 5b). The change in the ozone sensitivity regimes is consistent with (1) the decreased concentration in the simulated HNO_3 (Fig. S10a) due to less NO_2 reacting with OH, and (2) the increased H_2O_2 concentration (Fig. S10e) due to the reduced aerosol HO_2 uptake by aerosols. With a 50% reduction in AVOCs emissions, some transition areas of southern China are converted to VOC-limited areas (Fig. 5c). A relevant decrease in the H_2O_2 concentration is also derived in southern China and is attributed to the decrease in the calculated HO_2 concentration. When considering the combined reduction in NO_x and AVOCs emissions as well as the reduction in all anthropogenic emissions, the VOC-limited regions of southern China evolve towards a transition region or even a NO_x-limited region (Fig. 5d; Fig. S11a). In these two last cases, the changes in ozone sensitivity regimes are determined by the decrease in the calculated HNO_3 concentrations (Fig. S10 c-d). At the urban sites, the emission reduction does not modify the wintertime ozone sensitivity regimes (Fig. S12), which remain VOC-limited.

Summer conditions. In July, the changes in ozone regimes related to emission reductions are found mainly in VOC-limited areas and in their surroundings, due to consistent changes in H_2O_2 and HNO_3 (Fig. S13). With the reduction of NO_x emissions, the size of VOC-limited areas (Fig. 5e) shrinks and becomes a smaller fraction of the urbanized areas (Fig. 5f). At four urban sites (VOC-limited in *BASE* case), the ozone sensitivity of Beijing sites is converted to NO_x-limited (Fig. 5i). The sites of Shanghai (Fig. 5j) and Chengdu (Fig. 5l) are shifted to a Transition area. Only the Guangzhou site remains in a VOC-limited region (Fig. 5k). With the reduction in AVOCs emissions, the VOC-limited areas expand to the surroundings of the metropolitan areas (Fig. 5g). Finally, when considering the combined 50% reduction in the emissions of NO_x and AVOCs (*N+A* case; Fig. 5h) as well as the reduction of all other emitted species (*TOTAL* case; Fig. S11b), the pattern of calculated change in the ozone sensitivity is similar to the pattern corresponding to the NO_x emissions, with a smaller VOC-limited area

relative to the *BASE* case. In these cases, the sites of Beijing and Chengdu shift to a transition condition, while the Guangzhou and Shanghai sites remain under VOC-limited conditions.

3.2.2 Response of ozone concentrations to emission reduction

Figure 6 shows the changes in daytime (06:00 to 19:00 LST) surface ozone concentrations resulting from a 50% reduction of the NO_x and AVOCs emissions in January and July of 2018.

Winter conditions. In January, the 50% reduction in the NO_x emissions enhances the surface ozone concentrations, with the largest increase derived in the YRD and PRD regions by 15-33% (6-12 ppbv; Fig. 6a). During wintertime, a large part of China is under a VOC-sensitive regime. Therefore, the reduced titration of ozone by reduced NO concentrations (Fig. S14a; Fig. S2c) favors an increase in the ozone concentration. If AVOCs emissions are reduced by 50%, the surface ozone is reduced by 4-10% (2.0 to 8.0 ppbv; Fig. 6b) in the southern part of China. This ozone decrease is associated with the reduced concentration of HO_x radicals and hence a reduction in the ozone production by the HO_2 + NO reaction (Fig. S15a).

In the combined emission reduction case, the ozone response in VOC-limited areas follows the positive changes found in the NO_x-reduction case, with an ozone increase of 4-9% (3.0-7.5 ppbv; Fig. 6c) in North China and in some urban regions in South China. Simultaneously, a slight ozone decrease is derived along the southern coast of China (5-8% or 2.0-4.5 ppbv). In these areas, the ozone sensitivity is under the control of the NO_x. The ozone decrease is dominated by the negative ozone response to the AVOCs emission reduction. With further emission reduction of the other species, an ozone increase (4-6% or 3-5 ppbv; Fig. S4g) relative to the combined case is calculated in the southern part of China, resulting from the increased HO_2 radical (Fig. S4c) reacted with NO.

Summer conditions. In July, under the reduction in the NO_x emissions, an increase in the surface ozone concentration of up to 17% (10 ppbv; Fig. 6d) is calculated in the urbanized regions of NCP, YRD, and PRD. These areas are typically located in VOC-limited areas; thus, the ozone increase is explained by the reduced ozone titration (Fig. S14b). At the same time, in NO_x-limited areas, the calculated surface ozone concentration is reduced by 3-10% (2 to 8 ppbv), as a result of reduced photochemical formation under lower NO_x concentrations. With the reduction of AVOCs emissions, the surface ozone concentration decreases by 8-20% (8.0-12.0 ppbv; Fig. 6e) in whole areas of China. A spatial shift in the ozone decrease area, from the southern regions in winter to the northern regions in summer occurs under this condition; this change is consistent with the spatial distribution of the reduction in the mixing ratio of the HO_2 radical, which contributes to the ozone production by its reaction with nitric oxide (Fig. S15b).

In the combined emission reduction case, the surface ozone concentration decreases by up to 15% (12 ppbv; Fig. 6f) in NO_x-sensitive areas. In VOC-sensitive areas, the surface ozone concentration also decreases, which differs from the ozone changes during wintertime. This is explained by the fact that the loss of ozone due to NO_x titration is rapidly compensated by the

photochemically formation of ozone, since the ozone production rate during summertime is accelerated by the high temperature and photolysis rate (T. Wang et al., 2022). One exception can be found at the Guangzhou site, where ozone increases by 0.5 ppbv (1~2%; Fig. S16). This increase of ozone is consistent with the increase of OH radical and OVOCs at this site, which is related to the increasingly important role played by naturally emitted BVOCs species in the oxidation processes when anthropogenic emissions are reduced (see Sec. 3.3). When the emission reduction is applied to all species under consideration, the ozone changes (Fig. S4h) relative to the combined case are smaller than the changes in winter, due to a consistently smaller reduction in aerosol concentrations (see Sec. 3.2.3).

3.2.3. Response of aerosols to emission reduction

Figure 7 shows the changes in the average concentrations of secondary aerosol due to emission reduction in January and July of 2018.

Winter conditions. In January, the 50% reduction of NO_x leads to a large decrease in the aerosol load (10-18 μg m^{-3} or 12-20%; Fig. 7a) of central and southern China. The aerosol decrease predominantly results from the decrease in the NO_3^- abundance (Fig. S17a) linked to the reduced concentration of NO_2, followed by effect of NO_4^+ (Fig. S17b). A slight increase in the abundance of secondary organic aerosols (SOA) is derived in the urban areas of NCP, YRD, and PRD regions (1-2 μg m^{-3} or 3-5%; Fig. S17c), which is consistent with the increase in the level of oxidants, including ozone and OH radicals. With a 50% reduction of AVOCs emissions, the changes in the aerosol concentration are smaller than with the 50% reduction in NO_x emissions, with a decrease of less than 4% (5 μg m^{-3}; Fig. 7b), which predominantly results from the reduction in SOA (Fig. S18a). With a joint reduction in NO_x and AVOCs (Fig. 7c), the aerosol decrease is larger than the separated effect of the individual emissions decrease, as the increase in the concentration of SOA resulting from the reduced NO_x emissions is compensated by the reduced AVOCs emissions.

With a further reduction in other emissions, the decrease in the concentration of aerosol is deeply enhanced; this is the case for the concentration of NH_4^+ (919a), SO_4^{2-} (Fig. S19b), and NO_3^- particles (Fig. S19c). The concentration of the gas-phase precursors, NH_3 and SO_2, is considerably reduced, which affects the process of acid replacement (Meng et al., 2022) and hence the level of NO_3^-. In our model, the concentration of NO_2 and $PM_{2.5}$ is overestimated for the baseline conditions, which can possibly lead to an excessively high reduction in aerosol concentration, especially in the concentration of NO_3^-. This overestimation potentially affects the aerosol-related changes in ozone formation.

Summer conditions. In July, the decrease in aerosol load due to the emission reduction is much smaller than in winter. The reduction ranges from 1.5 to 5 μg m^{-3} (Fig. 7d), from 2 to 6 μg m^{-3} (Fig. 7e), from 4 to 7 μg m^{-3} (Fig. 7f) and from 8 to 10 μg m^{-3} (Fig. 7g), for the reduction in the NO_x, AVOCs, combined NO_x and AVOCs, and *TOTAL* emissions, respectively. Similar with the ozone changes, the simulated reductions in aerosols also undergo a spatial shift, from the southern part of China in winter to the northern China Plain in summer. This shift is consistent

with the calculated changes in oxidants, hydrocarbons, and other gaseous aerosol precursors. The higher decrease in the aerosols loads for the combined case also indicates that the reduction in AVOCs emission increases the efficiency of the aerosol decrease produced by the reduced NO_x emissions.

The aerosol effect on the ozone formation has been discussed in several modeling studies (Li et al., 2019; Liu et al., 2020; Dai et al., 2023). Our results show that the reduction in primary emissions results in a large decrease of aerosol concentrations. The major contribution to the aerosol decreases results from the reduction in NO_x emissions, with a strengthened effect when combined with a reduction in the AVOCs emissions. This decrease in the aerosol burden weakens the aerosol extinction effect and therefore enhances the photochemical formation rate of radicals and ozone. As shown in Fig. S20 a-d, the photolysis rate increases (by 5-20%) in southern and central China during winter due to the aerosol decrease induced by the emission reductions. The highest increase in photolysis rates results from the joint emission reduction in NO_x and AVOCs (Fig. S20c). The increase of the photolysis rates in summer is not as distinct as the increase during wintertime due to the more limited reduction of the aerosol burden during summer (Fig. S20e-h).

Further, the reduction in the aerosol burden lowers the aerosol uptake of NO_2 and HO_2 radicals, which indirectly enhances the mixing ratio of OH and HO_2 radicals (Dai et al., 2023). An increased level of HO_x (Fig. S4 a-d) following the emission reduction in NH_3 and SO_2 can be caused by the reduced aerosol uptake, associated with a large decrease in the calculated concentrations of NH_4^+ and SO_4^{2-}. In short, the reduction in the aerosol load is supportive of the ozone formation. Therefore, there is a need to consider the aerosol effect on ozone formation even with stringent emission reduction.

3.3. Changes in atmospheric oxidative capacity

The Atmospheric Oxidizing Capacity (*AOC*) is a parameter that characterizes the self-cleansing ability of the atmosphere (Liu et al., 2022). It is derived here as the rate at which carbon monoxide (CO), methane (CH_4), and non-methane hydrocarbons (NMHCs) are oxidized by atmospheric oxidants, including OH, O_3, and NO_3 (Xue et al., 2016; Dai et al., 2023). This parameter allows us to characterize the formation process of O_3 and can be used as an indicator to design mitigation policies for reducing ozone pollution.

The changes in the spatial distribution of daytime (06:00 to 19:00 LST) *AOC* resulting from the adopted 50% reduction in the emissions of ozone precursors for January and July of 2018 are depicted in Fig. 8.

Winter conditions. In January, the 50% reduction in NO_x emission leads to a decrease in daytime *AOC* of 10~20% in southern China and an increase of 10~18% in the urban areas, including the PRD, YRD and SCB regions (Fig. 8a). At the four city sites (Fig. 9 a-d), the increase in the daytime *AOC* is attributed to the enhanced contributions of the OH-related reactions, including the reactions of OH with alkenes, followed by the reaction of OH with

OVOCs and with aromatics. This daytime *AOC* increase is consistent with the enhanced level in the OH radical, alkenes, and OVOCs when NO_x emission reduced. During nighttime (20:00 to 05:00 LST), the reduction in NO_x emissions is responsible for an increase in *AOC* by up to 50% (Fig. S21a). A contribution to this increase is provided by the alkenes' ozonolysis, since the concentration of ozone (Fig. 6a) and of alkenes is enhanced (Fig. S9c). The largest increase in the alkene ozonolysis is derived at the sites of Shanghai from 31% to 40% (Fig. S22b). These results highlight the promoted oxidative processes associated with the NO_x emission reduction.

With the 50% reduction in AVOCs emissions, the daytime *AOC* is reduced in all the major regions of China (Fig. 8b), with the largest decreases occurring in the southern part of the country, with the largest decrease occurring at Guangzhou site (by 50%). This decrease in daytime *AOC* is mainly attributable to the reduced contribution from the reactions between OH and alkenes, followed by the reactions of OH with aromatics and with OVOCs. With a combined emission reduction in NO_x and AVOCs emissions (Fig. 8c) and with the additional reduction in the other emissions considered here (Fig. S23a), the distribution patterns of the changes in daytime *AOC* are similar to the patterns found in the *AVOCs* cases but are characterized by higher decreases in daytime *AOC*.

Summer conditions. During summertime, the decrease in daytime *AOC* is more pronounced than in wintertime. With the 50% reduction in NO_x emissions, daytime *AOC* decreases in large areas of China (ranging from 10% ~ 20%; Fig. 8d), while, in urban areas, an increase of is predicted, including the Guangzhou (8%; Fig. 9g), Shanghai (5%; Fig. 9f), and Chengdu (3%; Fig. 9h). However, at the Beijing site, the daytime value of *AOC* decreases (Fig. 9e), because of the shift in the ozone sensitivity regime from VOC-limited to NO_x-limited. During nighttime, the NO_x emission reduction also leads to an increase in *AOC* due to the alkene ozonolysis (Fig. S21b), with the largest increase derived at the Beijing site (from 10% to 14%; Fig. S22e).

With other emission reduction cases (AVOCs, *N+A*, and *TOTAL*; Fig. 8e-f; Fig. S23b), the daytime *AOC* decreases in the entire China, with more distinct decreases in North China relative to winter conditions. With the reduction in the AVOCs emissions, the relative decrease of daytime *AOC* is smaller than in winter, especially at the Guangzhou site (to 30%), indicating a more important secondary formation of VOC-related *AOC* during summer. When the emissions of NO_x and AVOCs are jointly reduced by 50%, the role of the reaction between OH and BVOCs in the determination of *AOC* is enhanced at the four city sites, with the largest increase (15%) found at the Guangzhou site. This increase results from the enhanced levels in OH radicals (Fig. 2c) and in biogenic VOCs species, such as isoprene (Fig. S24).

The distribution patterns of changes in daytime *AOC* due to emission reduction is to a large extent consistent with the changes in the mixing ratio of the OH radicals and the changes in the concentration of OVOCs, ozone, and SOA in both winter and summer. These consistent patterns suggest that the *AOC* is an appropriate indicator to characterize the changes in secondary pollutants attributed to emission reduction. One exception is found when considering the changes in the ozone concentration resulting from the reduction in the NO_x emission during winter. During this season, a comparison between the values of daytime *AOC*

and the changes in the ozone concentration (Fig. 5a) suggests that the change in daytime *AOC* reflects primarily the changes in the net production rate of odd oxygen (Fig. S25); this can be explained by the important role played by NO_2 in the wintertime formation of ozone.

4. Summary and Policy Implications

The model simulations performed in the present study explore the response of radicals, of ozone, and of the atmospheric oxidative processes to a 50% reduction in primary emissions of key pollutants. Our analysis provides insight into the changes affecting ozone chemistry and the oxidizing processes to be expected in response to future emission reduction.

In winter, as most geographical areas are VOC-limited (saturated in NO_x) a 50% reduction in NO_x emissions leads to an ozone concentration increase of up to 8-10 ppbv (15-25%) in all geographical regions of China; this increase results from of the reduced titration of ozone by nitric oxide. When combining this NO_x reduction with a 50% reduction in AVOCs emissions, the ozone enhancement found in the rural areas and resulting from the reduced NO_x is considerably reduced. However, in urban areas (VOC-limited situation), the ozone increase, although weakened, still exists (by 3.0-7.5 ppbv).

In summer, as most rural areas of China become NO_x-limited, the geographical regions covered by the ozone increase in response to the 50% reduction applied to the NO_x emissions shrink almost to the VOC-limited metropolitan areas. In these urban environments, the ozone increase reaches a maximum of 10 ppbv or 17%. When the NO_x emission reduction is combined with a 50% reduction in the VOC emissions, the increase in ozone almost disappears in all areas of China. This is explained by the significant decrease in ozone production resulting from the reduced level of hydrocarbons. However, in the areas where hydrocarbons are primarily of biological origin, the ozone concentration (i.e., linked to the photochemical degradation of isoprene) still slightly increases.

Paths to mitigation. We conclude this paper by highlighting a few chemical paths that should be considered when designing a mitigation policy for a reduction of ozone in the urban areas of China. Figure 10 presents a schematic description of the chemical mechanisms involved in the chemical production of atmospheric ozone and highlights how different reaction paths tend to change the ozone abundance in response to a reduction in NO_x and in anthropogenic VOC (AVOCs) emissions. This graph shows that a reduction in NO_x emissions tends to increase the ozone concentration by (1) reducing the rate of the $NO + O_3$ reaction (ozone titration); (2) by increasing the rate of the $HO_2 + NO$ reaction due to an increase in the HO_2 level associated with the reduced uptake of this radical by a lowered aerosol load; (3) by an increase in the atmospheric oxidizing capacity (*AOC*) through OH- and ozone-related reactions. The graph also shows that a decrease in AVOCs emissions tends (1) to reduce the level of the HO_x radical and hence the ozone production by the $HO_2 + NO$ reaction; (2) to enhance the level of HO_x due to the reduced aerosol uptake and (3) to reduce the *AOC* with a negative effect on the ozone concentration. The relative importance of these different chemical mechanisms varies with location and environmental conditions.

We conclude that, in winter when the background ozone concentration is low, the reduction of NO_x emissions tends to increase the level of near-surface ozone, while the reduction in AVOC emissions has the opposite effect. This conclusion applies both in rural and in urban areas. A combined reduction in the emissions of these two primary pollutants tends to decrease the level of ozone in rural areas, but to increase ozone in urban areas. Thus, in urban areas during winter, an effective approach to reduce the surface ozone concentration is through a strong limitation in the emissions of volatile organic compounds.

In summer when the ozone level is generally high, the reduction of NO_x emissions is an effective action to reduce the ozone concentration in rural areas, but this measure is counterproductive in the NO_x-saturated urban areas where ozone is controlled by VOCs. In fact, in urban areas during this season, the mechanisms involved in ozone mitigation are complex. For example, when NO_x emissions are reduced, the atmospheric OH concentration is enhanced because of its reduced destruction by NO_2. Following this increase in the OH concentration, an increase in the level of OVOCs, whose photolysis is an important source of HO_x radicals, also leads to accelerated ozone production and further amplifies the oxidation of VOCs. In addition, the increase in *AOC*, linked to the reaction of OH and ozone with alkenes and the reactions of OH with OVOCs also contribute to an increase in the ozone production. Further, the reduction in the aerosol load resulting from a reduction in the emissions of aerosol precursors promotes the ozone formation by decreasing the aerosol extinction and by reducing the uptake of HO_2. If combined with a 50% reduction in AVOCs, the increase in the OVOC concentrations and in *AOC*, resulting from due to reduced NO_x emissions, can be offset. However, the aerosol-related promotion of the level of OH and HO_2 radicals can be enhanced, highlighting the complexity of summertime ozone mitigation in urban areas.

Table 2 provides quantitative information on the response of ozone at different urban locations for January and July. In urban areas, the reduction in the level of surface ozone requires a reduction in the emissions of anthropogenic VOCs. However, for practical reasons, a 50% reduction in AVOCs emissions, as assumed in our study, is difficult to implement over a short period of time. With the known contribution of the VOCs-related reactions to the *AOC*, the reduction in the emissions of alkenes, aromatics, and unsaturated OVOCs, especially methanol and ethanol, should be a priority. The development of efficient mitigation strategies based on the reduction of AVOCs emissions requires, however, more detailed investigations on the reactivity of individual VOCs and on their potential impact on the ozone formation.

Code and data availability. The WRF-Chem model is publicly available at https://www2.mmm.ucar.edu/wrf/users/. The modified code in the WRF-Chem model is available upon request to the corresponding author. The air quality data at surface stations are publicly available at the website of the Ministry of Ecology and Environment of the People's Republic of China at http://english.mee.gov.cn/.

Author contributions. JD and GB designed the structure of the manuscript, performed the numerical experiments, analyzed the results, and wrote the manuscript. JD analyzed the data and established the figures. All co-authors provided comments and reviewed the manuscript.

Competing interests. The authors declare that they have no conflict of interest.

Acknowledgments. The present joint Sino-German study was supported by the German Research Foundation (Deutsche Forschungs Gemeinschaft DFG), the National Science Foundation of China (NSFC) under Air-Changes grant no. 4487-20203, the Research Grants Council– University Grants Committee (grant no. T24-504/17-N) and the NSFC (grant no.42293322). The National Center for Atmospheric Research (NCAR) is sponsored by the US National Science Foundation. We would like to acknowledge the high-performance computing support from NCAR Cheyenne.

References

China Air 2023, Air Pollution Prevention and Control Progress in Chinese Cities. http://www.allaboutair.cn/uploads/231027/ChinaAir2023EN.pdf

Dai, J., Brasseur, G. P., Vrekoussis, M., Kanakidou, M., Qu, K., Zhang, Y., Zhang, H., and Wang, T.: The atmospheric oxidizing capacity in China – Part 1: Roles of different photochemical processes, Atmos. Chem. Phys., 23, 14127–14158, https://doi.org/10.5194/acp-23-14127-2023, 2023.

Emmons, L. K., Walters, S., Hess, P. G., Lamarque, J.-F., Pfister, G. G., Fillmore, D., Granier, C., Guenther, A., Kinnison, D., Laepple, T., Orlando, J., Tie, X., Tyndall, G., Wiedinmyer, C., Baughcum, S. L., and Kloster, S.: Description and evaluation of the Model for Ozone and Related chemical Tracers, version 4 (MOZART-4), Geosci. Model Dev., 3, 43–67, https://doi.org/10.5194/gmd-3-43-2010, 2010.

Jacob, D. J., Horowitz, L. W., Munger, J. W., Heikes, B. G., Dickerson, R. R., Artz, R. S., and Keene, W. C.: Seasonal transition from NOx - to hydrocarbon-limited conditions for ozone production over the eastern United States in September, J. Geophys. Res.-Atmo., 100, 9315–9324, https://doi.org/10.1029/94JD03125, 1995.

Knote, C., Hodzic, A., Jimenez, J. L., Volkamer, R., Orlando, J. J., Baidar, S., Brioude, J., Fast, J., Gentner, D. R., Goldstein, A. H., Hayes, P. L., Knighton, W. B., Oetjen, H., Setyan, A., Stark, H., Thalman, R., Tyndall, G., Washenfelder, R., Waxman, E., and Zhang, Q.: Simulation of semi-explicit mechanisms of SOA formation from glyoxal in aerosol in a 3-D model, Atmos. Chem. Phys., 14, 6213–6239, https://doi.org/10.5194/acp-14-6213-2014, 2014.

Li, B., Ho, S.S.H., Li, X., Guo, L., Chen, A., Hu, L., Yang, Y., Chen, D., Lin, A., Fang, X., A comprehensive review on anthropogenic volatile organic compounds (VOCs) emission estimates in China: comparison and outlook. Environ. Int. 156, 106710, https://doi.org/10.1016/j.envint.2021.106710, 2021.

Li, C., Liu, Y., Cheng, B., Zhang, Y., Liu, X., Qu, Y., Feng, M.: A comprehensive investigation on volatile organic compounds (VOCs) in 2018 in Beijing, China: Characteristics, sources and behaviors in response to O3 formation. Sci. Total Environ, 806, 150247https://doi.org/10.1016/j.scitotenv.2021.150247, 2022.

Li, J., Xie, X., Li, L., Wang, X., Wang, H., Jing, S. A., Hu, J.: Fate of Oxygenated Volatile Organic Compounds in the Yangtze River Delta Region: Source Contributions and Impacts on the Atmospheric Oxidation Capacity. Environ. Sci., Technol., 56(16), 11212-11224.https://doi.org/10.1021/acs.est.2c00038, 2022.

Li, K., Jacob, D. J., Liao, H., Shen, L., Zhang, Q., Bates, K. H.: Anthropogenic drivers of 2013−2017 trends in summer surface ozone in China. Proc. Natl. Acad. Sci., 116 (2), 422−427, https://doi.org/10.1073/pnas.1812168116, 2019.

Li, K., Jacob, D. J., Liao, H., Qiu, Y., Shen, L., Zhai, S., Kuk, S. K.: Ozone pollution in the North China Plain spreading into the late-winter haze season. Proc. Natl. Acad. Sci., 118(10), e2015797118, https://doi.org/10.1073/pnas.2015797118, 2021.

Liu, T., Hong, Y., Li, M., Xu, L., Chen, J., Bian, Y., Yang, C., Dan, Y., Zhang, Y., Xue, L., Zhao, M., Huang, Z., and Wang, H.: Atmospheric oxidation capacity and ozone pollution mechanism in a coastal city of southeastern China: analysis of a typical photochemical episode by an observation-based model, Atmos. Chem. Phys., 22, 2173–2190, https://doi.org/10.5194/acp-22-2173-2022, 2022.

Liu, Y., Geng, G., Cheng, J., Liu, Y., Xiao, Q., Liu, L., Zhang, Q.: Drivers of Increasing Ozone during the Two Phases of Clean Air Actions in China 2013–2020. Environ. Sci., Technol., https://doi.org/10.1021/acs.est.3c00054, 2023

Liu, Y., and Wang Tao: Worsening urban ozone pollution in China from 2013 to 2017 – Part 2: The effects of emission changes and implications for multi-pollutant control, Atmos. Chem. Phys., 20, 6323-6337, https://doi.org/10.5194/acp-206323, 2020.

Meng, F., Zhang, Y., Kang, J., Heal, M. R., Reis, S., Wang, M., Liu, L., Wang, K., Yu, S., Li, P., Wei, J., Hou, Y., Zhang, Y., Liu, X., Cui, Z., Xu, W., and Zhang, F.: Trends in secondary inorganic aerosol pollution in China and its responses to emission controls of precursors in wintertime, Atmos. Chem. Phys., 22, 6291–6308, https://doi.org/10.5194/acp-22-6291-2022, 2022.

Ou, J., Yuan, Z., Zheng, J., Huang, Z., Shao, M., Li, Z., Louie, P. K.: Ambient ozone control in a photochemically active region: short-term despiking or long-term attainment? Environ. Sci., Technol., *50* (11), 5720-5728, https://doi.org/10.1021/acs.est.6b00345, 2016.

Skamarock, W.C., Klemp, J.B., Dudhia, J., Gill, D.O., Liu, Z., Berner, J., Wang, W., Powers, J.G., Duda, M.G., Barker, D.M.: A Description of the Advanced Research WRF Model Version 4; Mesoscale and Microscale Meteorology Laboratory NCAR: Boulder, CO, USA, 2019.

Song, H., Lu, K., Dong, H., Tan, Z., Chen, S., Zeng, L., Zhang, Y.: Reduced aerosol uptake of hydroperoxyl radical may increase the sensitivity of ozone production to volatile organic compounds. Environ. Sci., Technol. Lett., 9(1), 22-29. https://doi.org/10.1021/acs.estlett.1c00893, 2021.

Tan, Z., Lu, K., Hofzumahaus, A., Fuchs, H., Bohn, B., Holland, F., Liu, Y., Rohrer, F., Shao, M., Sun, K., Wu, Y., Zeng, L., Zhang, Y., Zou, Q., Kiendler-Scharr, A., Wahner, A., and Zhang, Y.: Experimental budgets of OH, HO_2, and RO_2 radicals and implications for ozone

formation in the Pearl River Delta in China 2014, Atmos. Chem. Phys., 19, 7129–7150, https://doi.org/10.5194/acp-19-7129-2019, 2019.

Tan, Z., Lu, K., Ma, X., Chen, S., He, L., Huang, X., Zhang, Y.: Multiple Impacts of Aerosols on O3 Production Are Largely Compensated: A Case Study Shenzhen, China. Environ. Sci., Technol., 56(24), 17569-17580, https://doi.org/10.1021/acs.est.2c06217, 2022.

Tonnesen, G. S., and R. L. Dennis.: Analysis of radical propagation efficiency to assess ozone sensitivity to hydrocarbons and NO_x: 2. Long-lived species as indicators of ozone concentration sensitivity, *J. Geophys. Res.*, 105(D7), 9227–9241, https://doi.org/10.1029/1999JD900372, 2000.

Wang, J, Zhang Y, Xiao S, Wu Z, Wang X.: Ozone Formation at a Suburban Site in the Pearl River Delta Region, China: Role of Biogenic Volatile Organic Compounds. Atmosphere, 14 (4):609. https://doi.org/10.3390/atmos14040609, 2023.

Wang, T., Xue, L., Feng, Z., Dai, J., Zhang, Y., Tan, Y.: Ground-level ozone pollution in China: a synthesis of recent findings on influencing factors and impacts. Environ. Res. Letters, 17(6), 063003. https://doi.org/10.1088/1748-9326/ac69fe, 2022.

Wang, W., van der A, R., Ding, J., van Weele, M., and Cheng, T.: Spatial and temporal changes of the ozone sensitivity in China based on satellite and ground-based observations, Atmos. Chem. Phys., 21, 7253–7269, https://doi.org/10.5194/acp-21-7253-2021, 2021.

Wang, W., Yuan, B., Peng, Y., Su, H., Cheng, Y., Yang, S., Wu, C., Qi, J., Bao, F., Huangfu, Y., Wang, C., Ye, C., Wang, Z., Wang, B., Wang, X., Song, W., Hu, W., Cheng, P., Zhu, M., Zheng, J., and Shao, M.: Direct observations indicate photodegradable oxygenated volatile organic compounds (OVOCs) as larger contributors to radicals and ozone production in the atmosphere, Atmos. Chem. Phys., 22, 4117–4128, https://doi.org/10.5194/acp-22-4117-2022, 2022.

Xue, L., Gu, R., Wang, T., Wang, X., Saunders, S., Blake, D., Louie, P. K. K., Luk, C. W. Y., Simpson, I., Xu, Z., Wang, Z., Gao, Y., Lee, S., Mellouki, A., and Wang, W.: Oxidative capacity and radical chemistry in the polluted atmosphere of Hong Kong and Pearl River Delta region: analysis of a severe photochemical smog episode, Atmos. Chem. Phys., 16, 9891–9903, https://doi.org/10.5194/acp-16-9891-2016, 2016.

Yang, G., Liu, Y., Li, X. Spatiotemporal distribution of ground-level ozone in China at a city level. Sci Rep 10, 7229, https://doi.org/10.1038/s41598-020-64111-3, 2020.

Zaveri, R. A., R. C. Easter, J. D. Fast, and L. K. Peters, Model for Simulating Aerosol Interactions and Chemistry (MOSAIC), J. Geophys. Res., 113, D13204, doi:10.1029/2007JD008782, 2008

Zhang, Y., Dai, J., Li, Q., Chen, T., Mu, J., Brasseur, G., Wang, T., Xue, L.: Biogenic volatile organic compounds enhance ozone production and complicate control efforts: Insights from long-term observations in Hong Kong. Atmos. Environ., 309, 119917, https://doi.org/10.1016/j.atmosenv.2023.119917, 2023.

Zhao, X., Zhou, W., and Han, L.: Human activities and urban air pollution in Chinese mega city: An insight of ozone weekend effect in Beijing, Phys Chem Earth Pt. A/B/C, 110, 109–116, https://doi.org/10.1016/j.pce.2018.11.005, 2019.

Zheng, B., Tong, D., Li, M., Liu, F., Hong, C., Geng, G., Li, H., Li, X., Peng, L., Qi, J., Yan, L., Zhang, Y., Zhao, H., Zheng, Y., He, K., and Zhang, Q.: Trends in China's anthropogenic emissions since 2010 as the consequence of clean air actions, Atmos. Chem. Phys., 18, 14095–14111, https://doi.org/10.5194/acp-18-14095-2018, 2018

Zhu, S., Ma, J., Wang, S., Sun, S., Wang, P., Zhang, H.: Shifts of formation regimes and increases of atmospheric oxidation led to ozone increase in North China Plain and Yangtze River Delta from 2016 to 2019. J. Geophys. Res.: Atmos., e2022JD038373, https://doi.org/10.1029/2022JD038373, 2023.

Table 1. Sensitivity experiments

Model Experiments	Description
BASE	Without emission reduction
NOx	With emission reduction in NO_x[a] by a factor of 2
AVOCs	With emission reduction in anthropogenic VOCs[a] by a factor of 2
N+A	With emission reduction in NO_x[a] and anthropogenic VOCs[a] by a factor of 2
TOTAL	With emission reduction in all species[a] by a factor of 2

[a] Relevant species is shown in Sect. 2.1 and Table S1 in Supplementary Materials.

Table 2. Ozone changes due to reduction in emissions (in percentage)

Location	Sites name	Ozone changes in winter condition (Mean ± SD)			
		NOx[a]	*AVOCs*[b]	*N+A*[c]	*TOTAL*[d]
North	Beijing	25.0 ± 25.2[e]	-2.5 ± 1.3	22.0 ± 32.8	20.0 ± 19.5
East	Shanghai	33.2 ± 35.3	-18.2 ± 13.5	21.8 ± 20.5	22.7 ± 18.8
South	Guangzhou	21.4 ± 22.6	-17.1 ± 11.2	7.1 ± 3.2	10.0 ± 3.5
West	Chengdu	21.3 ± 23.8	-9.4 ± 8.5	14.1 ± 8.3	20.3 ± 13.5
Location	Sites name	Ozone changes in summer condition (Mean ± SD)			
		NOx	*AVOCs*	*N+A*	*TOTAL*
North	Beijing	6.4 ± 3.8	-21.8 ± 19.2	-5.5 ± 4.2	-7.3 ± 5.0
East	Shanghai	17.1 ± 12.8	-22.9 ± 20.8	-2.9 ± 2.1	-2.6 ± 1.5
South	Guangzhou	15.0 ± 13.1	-14.5 ± 13.5	1.3 ± 1.0	1.3 ± 0.9
West	Chengdu	5.5 ± 4.5	-14.5 ± 10.2	-5.5 ± 2.0	-4.5 ± 1.9

a-d. Sensitivity cases with a 50% reduction in the emissions of NO_x (*NOx*), AVOCs (*AVOCs*), NOx and AVOCs (*N+A*), and other species (NOx, AVOCs, CO, NH_3, SO_2) under consideration (*TOTAL*).

e. Values are displayed in the average ozone changes during daytime (06:00-19:00) in percentage with the standard deviation as the error bar. (ozone changes = (case value – base value)/base value ×100).

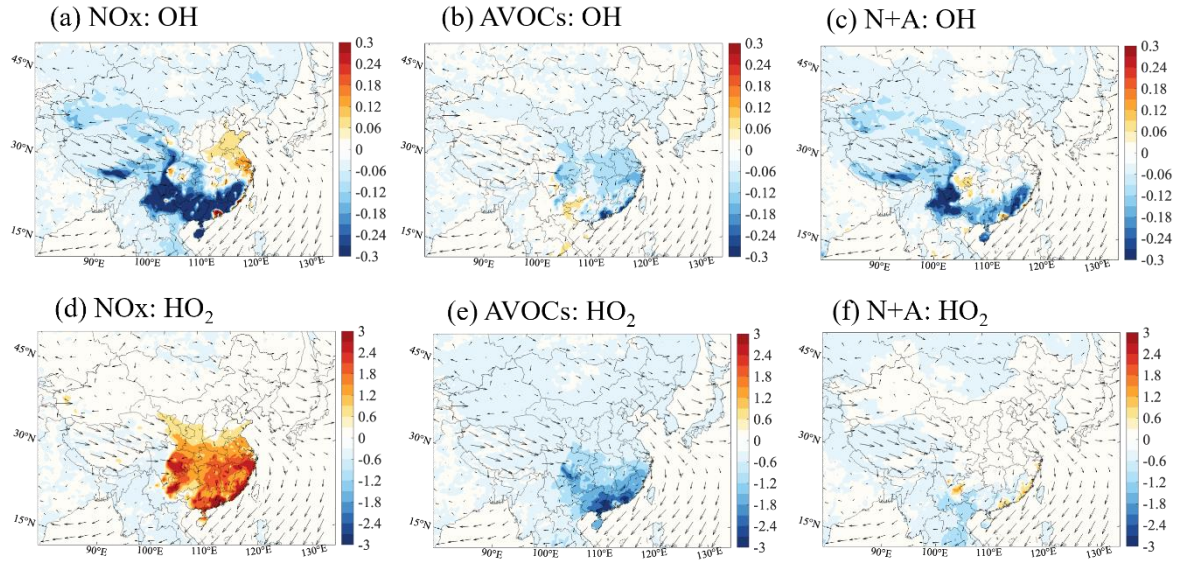

Figure 1. Changes in the monthly-averaged daytime (06:00 to 19:00 LST) surface mixing ratio of OH radical (a-c, Unit: 0.1 pptv) and HO_2 radical (d-f, Unit: pptv) response to a 50% reduction in the emissions of NO_x (a, d; *NOx* case), anthropogenic VOCs (b, e; *AVOCs* case) and in NO_x and AVOCs (c, f; *N+A* case) relative to *BASE* case for January of 2018. Arrows represent the wind speed and wind direction.

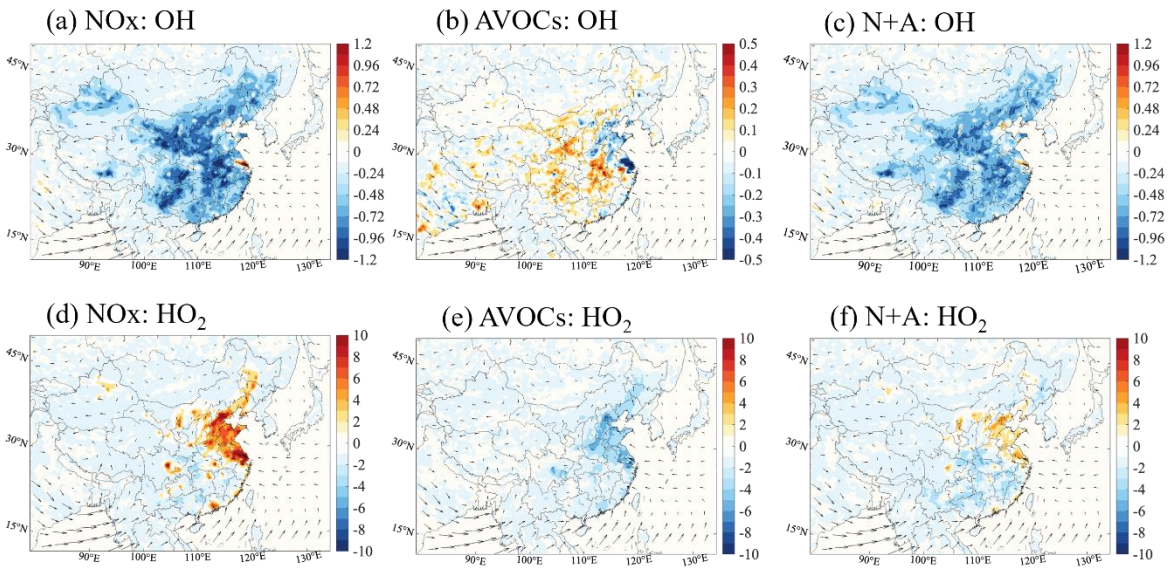

Figure 2. Same as Fig.1 but for July of 2018. Notice the inconsistency in the scale of Figure 2b.

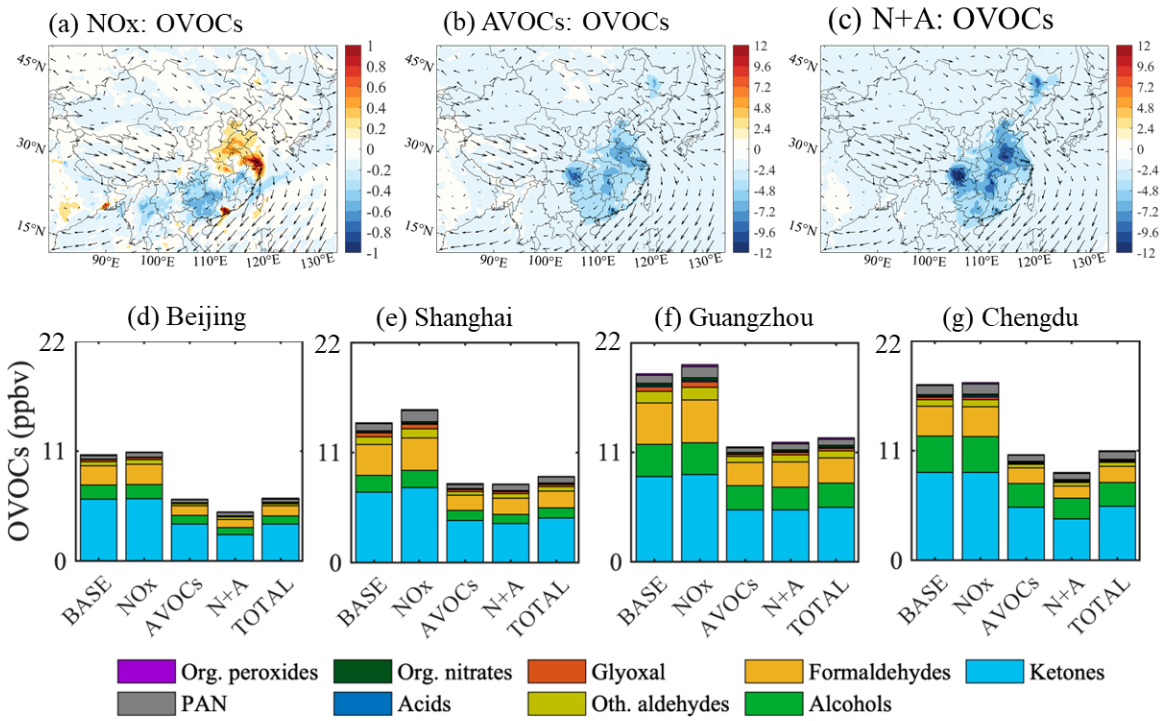

Figure 3. Changes in the monthly-averaged surface concentration of total oxidized VOCs (OVOCs) for January 2018. (a-c) Changes in the concentration of total OVOCs (Unit: ppbv) response to the reduction in NOx, AVOCs, and combined NOx and AVOCs emissions relative to the *BASE* case. (d-g) Averaged concentration of OVOC contributed by different species at four city sites (Beijing, Shanghai, Guangzhou, and Chengdu) in China in five simulated cases (*BASE*, *NOx*, *AVOCs*, *N+A*, and *TOTAL* cases). Arrows in a-c represent the wind speed and wind direction. Notice the inconsistency in the scale of Figure 3a.

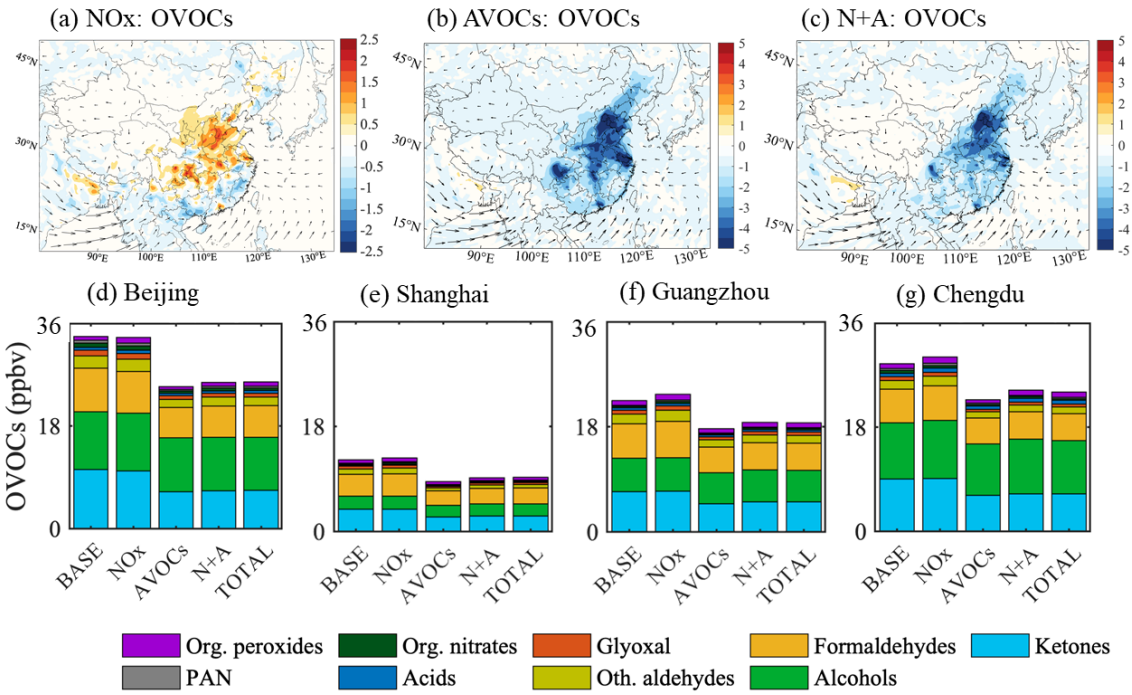

Figure 4. Same as Fig.3 but for July of 2018. Notice the inconsistency in the scale of Figure 4a.

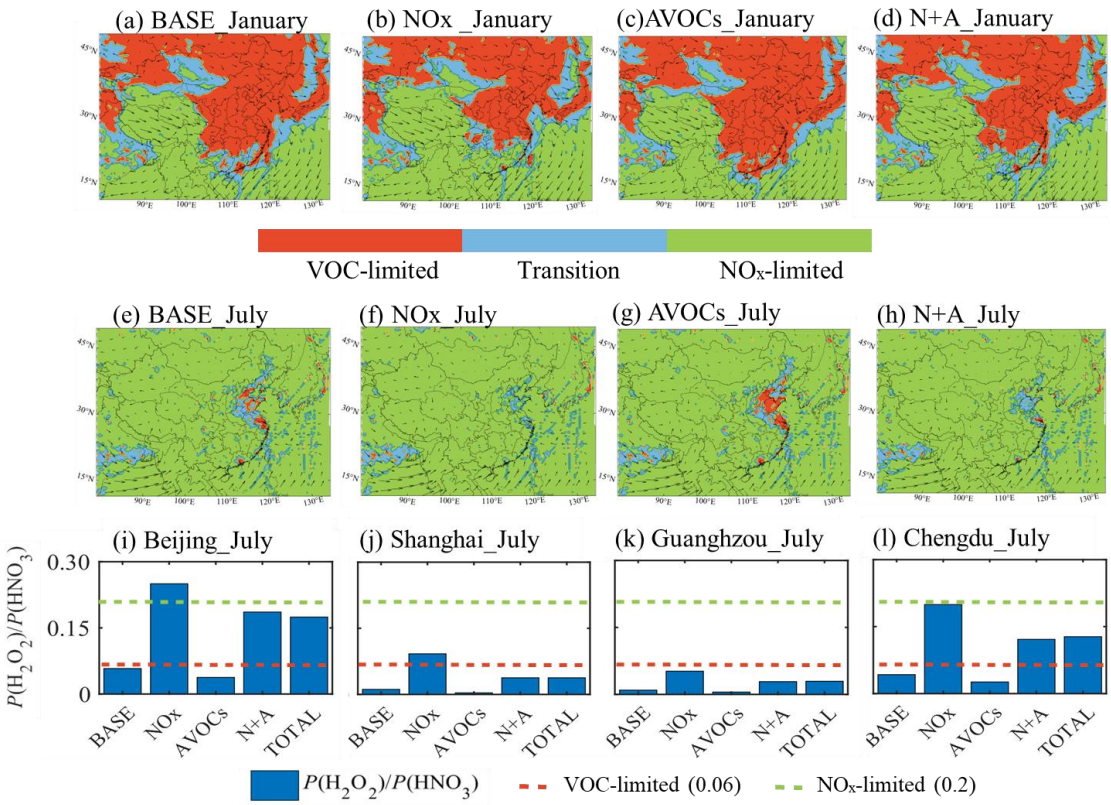

Figure 5. Ozone sensitivity regimes and their changes due to emission reduction. (a-h) Display of regions in which ozone production is limited by the availability of nitrogen oxides (NO_x-limited, in green), and volatile organic components (VOC-limited, in red) under the emissions in case of *BASE*, *NOx*, *AVOCs*, and *N+A* conditions in January (a-d) and July (e-h) of 2018. The regions where ozone production is controlled by the availability of both NO_x and VOCs (transition) are shown in blue. (i-l) The daytime (06:00 to 19:00 LST) value of the ratio between the production rate of hydrogen peroxide (H_2O_2) and nitric acid (HNO_3) [$P(H_2O_2)/P(HNO_3)$] at four city sites (Beijing, Shanghai, Chengdu, Guangzhou) in China in the five simulated cases for July 2018.

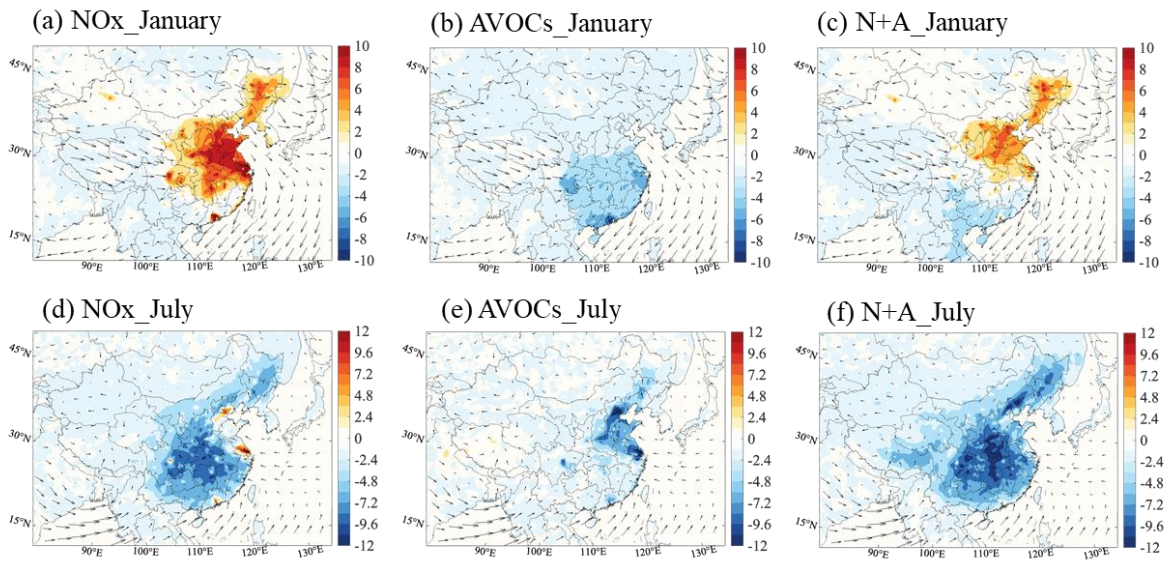

Figure 6. Changes in the monthly-averaged daytime surface ozone concentration (Unit: pptv) response to a 50% reduction in NO_x emissions (*NOx* case), in anthropogenic VOCs (AVOCs) emissions (*AVOCs* case) and in combined NO_x and AVOCs emissions (*N+A* case) relative to *BASE* case for January (a-c) and July (d-f) 2018. Arrows represent the wind speed and wind direction.

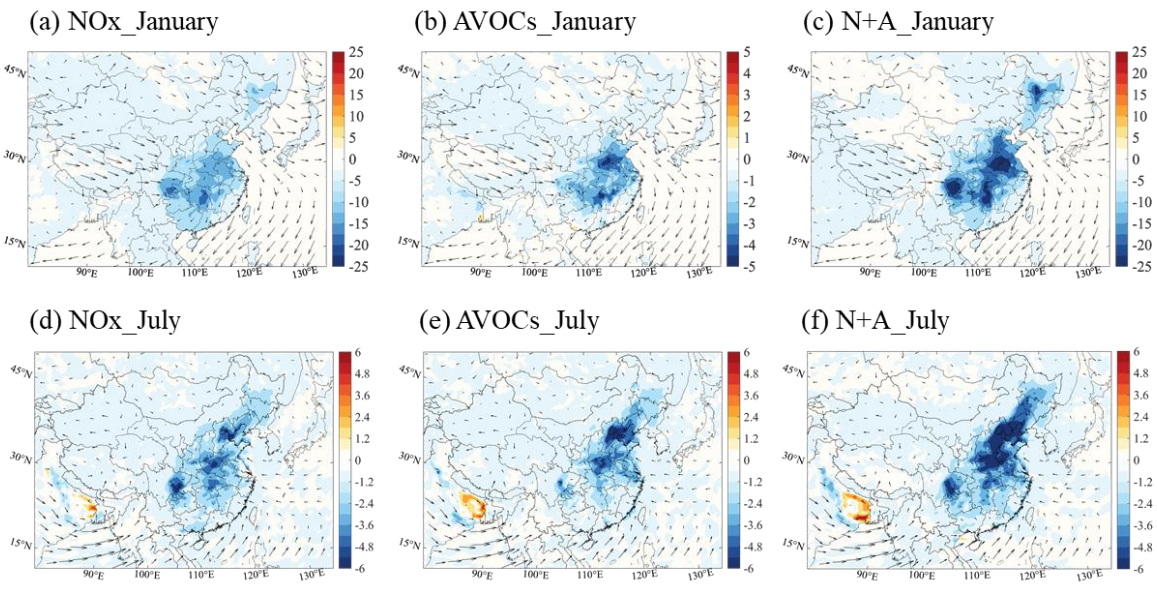

Figure 7. Changes in the monthly-averaged surface concentration of fine particulate aerosol (Unit: μg m^{-3}) in response to *NOx* (a, d), *AVOCs* (b, e) and *N+A* case (c, f) relative to *BASE* case for January (a-c) and July (d-f) 2018. Arrows represent the wind speed and wind direction. Notice the inconsistency in the scale of Figure 7b.

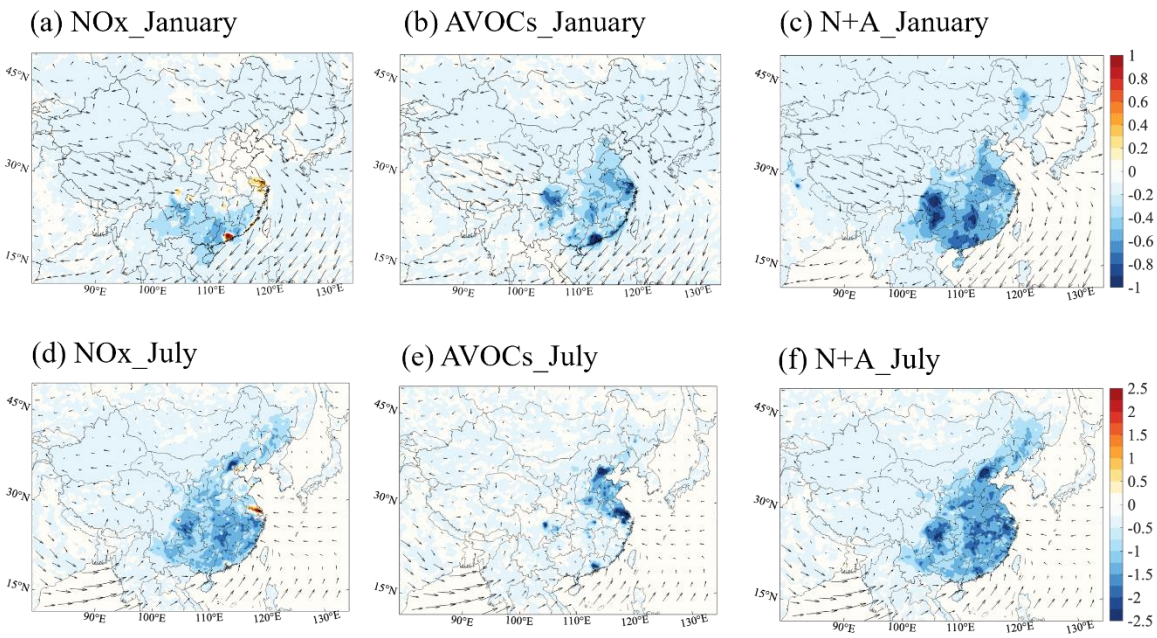

Figure 8. Changes in the monthly-averaged daytime value of atmospheric oxidizing capacity (*AOC*, Unit: 10^7 molec. cm^{-3} s^{-1}) response to NO_x (a, d), *AVOCs* (b, e), and *N+A* (c, f) cases relative to *BASE* case for January (a-c) and July (d-f) 2018.

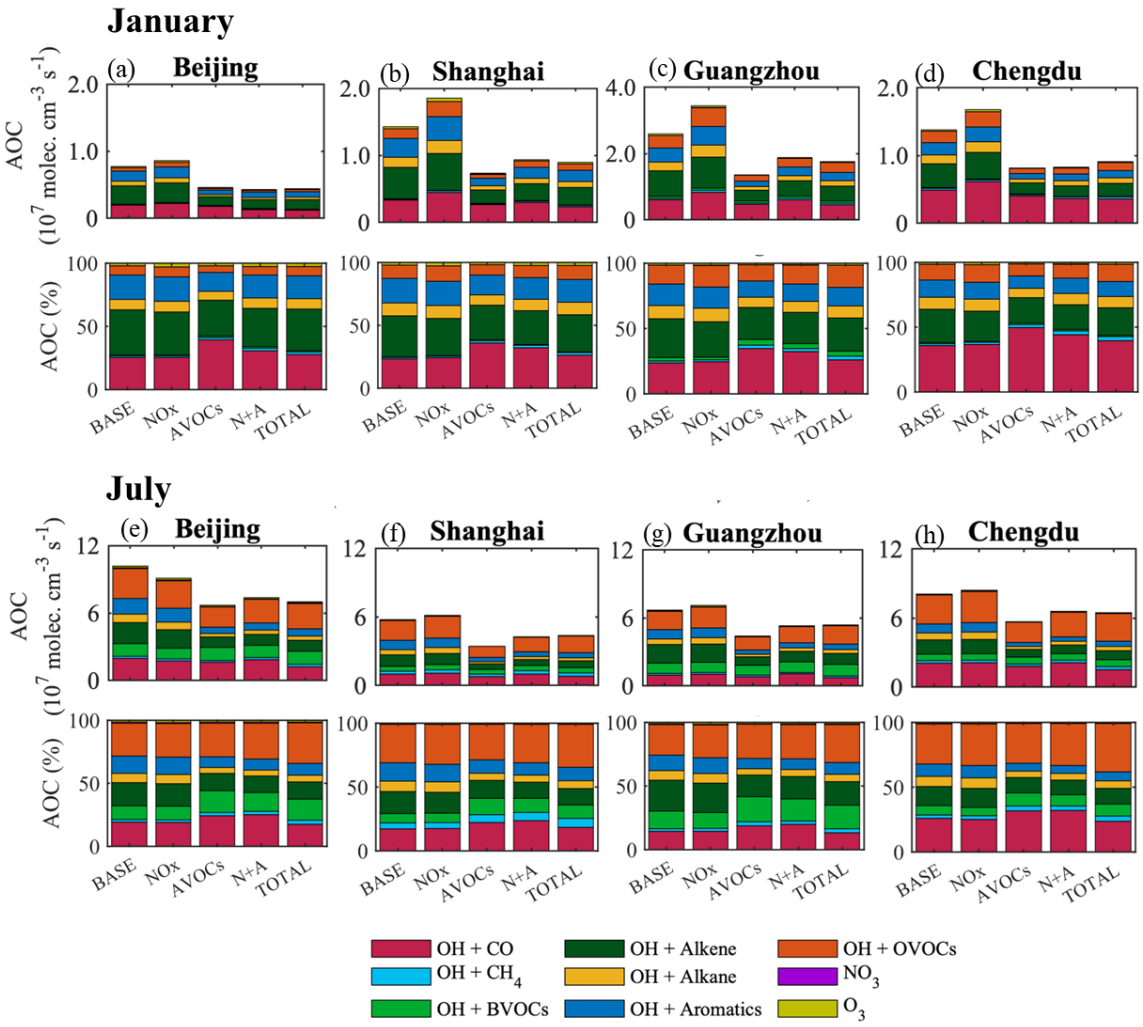

Figure 9. Monthly-averaged value (Unit: 10^7 molec. cm^{-3} s^{-1}) and relative terms (Unit: %) of daytime *AOC* at the sites of Beijing (a, e), Shanghai (b, f), Guangzhou (c, g), and Chengdu (d, h) in five simulated cases (*BASE*, *NOx*, *AVOCs*, *N+A*, *TOTAL* cases) in January (a-d) and July (e-h) of 2018. Notice the inconsistency in the scale of Figure 9c.

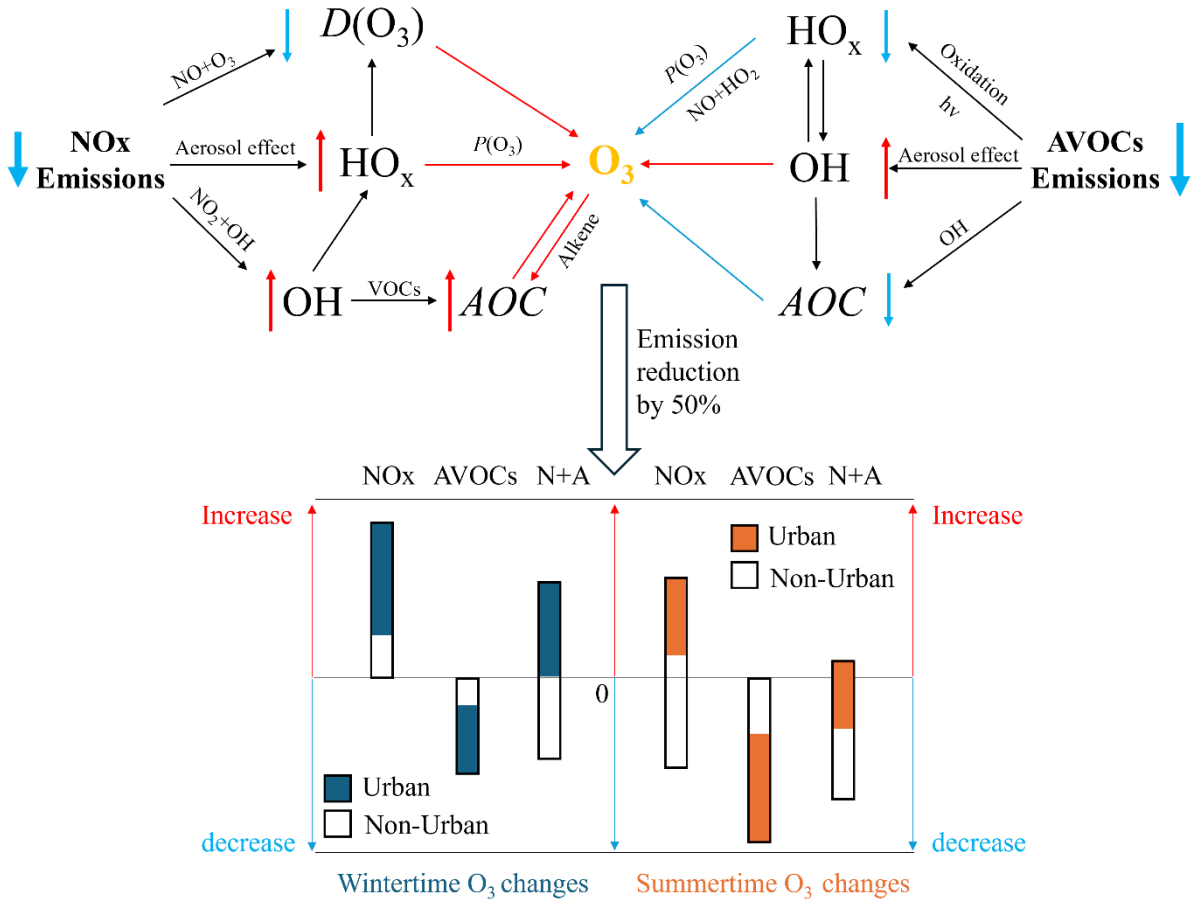

1150

Figure 10. Schematics show the responses of oxidative processes, associated with ozone formation, to the reduction in primary emissions of NO_x and AVOCs in urban areas (VOC-limited) in winter and summer. Arrows besides the chemicals represent the changes associated
1155 with the reduction in emission. (decrease trend shown in blue; increase trend shown in red) Blue and red arrows closing to O_3 represent the positive and negative contributions to the ozone formations. *AOC*, $P(O_3)$, and $D(O_3)$ are the abbreviations of the Atmospheric Oxidative Capacity, production of ozone, and destruction of ozone. Bar figure shows the ranges of ozone changes in whole of China (black bar), in non-urban areas (white part in the bar), and in urban
1160 areas (colored part in the bar) in three emissions cases (*NOx*, *AVOCs*, and *N+A* represent the case with emission reduction in NO_x, Anthropogenic VOCs (AVOCs), and the combined NO_x and AVOCs emissions, respectively) relative to *BASE* cases in winter and summer conditions.